The unique role of pore walls nanostructurization in the intrachannel photo-ATRP for fine-tuning PMMA tacticity

Paulina Maksym,*[ab] Roksana Bernat,[bc] Kajetan Koperwas,[bd] Marcin Wojtyniak, [e]Julita Piecha,[bd] Barbara Hachuła,[bc] Monika Geppert-Rybczyńska,[bc] Agnieszka Brzózka,[f] Grzegorz D. Sulka,[f] Magdalena Tarnacka,[bd] Marian Paluch,[bd] and Kamil Kamiński[bd]

[a.] *Institute of Materials Engineering, University of Silesia, 75 Pulku Piechoty 1a Street, 41-500 Chorzow, Poland*
[b.] *Silesian Center of Education and Interdisciplinary Research, University of Silesia, 75 Pulku Piechoty 1A Street, 41-500 Chorzow, Poland*
[c.] *Institute of Chemistry, University of Silesia, Szkolna 9 Street, 40-007 Katowice, Poland*
[d.] *Institute of Physics, University of Silesia, 75 Pulku Piechoty 1 Street, 41-500 Chorzow, Poland*
[e.] *Institute of Physics – Center for Science and Education, Silesian University of Technology, Krasińskiego 8, 40-019 Katowice, Poland*
[f.] *Department of Physical Chemistry and Electrochemistry, Faculty of Chemistry, Jagiellonian University, Gronostajowa 2 Street, 30-387 Krakow, Poland*

Supplementary Information

Table of contents

Materials

Ethyl α-bromoisobutyrate (EBiB, 98%, Sigma Aldrich), 1-naphthalene-10-phenoxazine (PC1, ≥97%, Sigma Aldrich), perylene (PC2, >99%, Sigma Aldrich), 3,7-Di(4-biphenyl) 1-naphthalene-10-phenoxazine (PC1, ≥97%, Sigma Aldrich), glycidyl methacrylate (GMA, ≥97%, Sigma Aldrich), anisole (anhydrous, 99.7%, Sigma Aldrich), N,N-Dimethylformamide (DMF, anhydrous, 99.8%, Sigma Aldrich), methanol (98%, Chempur), dimethyl sulfoxide (DMSO, 98%, Chempur), chloroform (98.5%, Chempur), chloroform-*d* (Sigma Aldrich) were used as received. Methyl methacrylate (MMA, >99%, Sigma Aldrich) was passed through a neutral alumina column to remove inhibitor.

Confined photo-ATRP polymerizations were carried out inside AAO-based hard confinement systems of uniaxial channels (open from both sides) and well defined pore arragements. Membranes of conical and modulated pore shapes were prepared according to procedure described in Ref [1]and Ref [2], respectively. Membranes of spherical pore shape were supplied from InRedox. Details concerning membranes characteristics can be found at the Webpage of the producer and collected in Table S1.[3]

We used following type of mesoreactors (see Scheme 1, main manuscript):

- type 1 – commercial, regularly ordered spherical pores (d=10, 35, and 160 nm);
- type 2 – self-produced, regularly ordered conical pores (d=35 nm);
- type 3 - self-produced, regularly ordered pores of modulated pore diameter (19<d<28nm).

Table S1. Detailed characteristics of Type 1 AAO-based templates

Pore diameter [nm]	Format/size [mm]	Thickness [μm]	Porosity [%]	Pore density [cm^{-2}]
160±20	10±0.1	50±2	16±3	8×10^{8}
35±4	13	50±2	12±2	1×10^{10}
10±3	10±0.1	50±2	12±2	1.6×10^{11}

Instruments

Fourier transform infrared spectroscopy (FT-IR) measurements were performed using a Nicolet iS50 FT-IR spectrometer (Thermo Scientific) equipped with an attenuated total reflectance (ATR) mode setup in the spectral range of 400 to 4000 cm^{-1}. FT-IR spectra were recorded with the spectral resolution of 4 cm^{-1} and 32 co-added scans for each spectrum.

^{1}H NMR spectra were collected on Bruker Ascend 500 MHz spectrometer for the samples in $CDCl_3$ at 25 °C.

Molecular weights (M_n) and dispersities (Đ) of produced polymers were determined by Size Exclusion Chromatography (SEC) with a Viscotec GPC Max VR 2001 and a Viscotec TDA 305 triple detection containing refractometer, viscosimeter and low angle laser light

scattering. The OmniSec 5.12 was used for data processing. Two D6000M (General Mixed Org 300x8mm) and Dguard (Org Guard Col 10x4.6mm) columns were used for separation. The measurements were carried out in DMF with LiBr (10 mmol) as the solvent at 40 °C with a flow rate of 0.7 mL/min.

UV-VIS measurements were performed using UV-VIS-NIR Microspectrophotometer from CRAIC Technologies equipped with halogen lamp and Zeiss 15x objective. The experiments were performed at room temperature and ambient pressure in the transmission geometry. The UV-VIS spectra of the other samples were obtained using UV-Vis Ratio Beam spectrophotometer from Hitachi (U-1900) equipped with standard UV quartz cuvettes.

Light equipment (Thorlabs): 365 nm 880 mW (Min) Mounted LED 1000 mA, Adjustable Collimation Adapter with Ø1" Lens AR Coating: 350 - 700 nm, T-Cube LED Driver 1200 mA Max Drive Current (Power Supply Not Included), 15 V 2.4 A Power Supply Unit with 3.5 mm Jack Connector for One K- or T-Cube, Slip Ring for SM1 Lens Tubes and C-Mount Extension Tubes</br>8-32 Tap, Ø1/2" Post Holder Spring-Loaded Hex-Locking Thumbscrew L = 3", Rotating Clamp for Ø1/2" to Ø6 mm Posts 360° Continuously Adjustable 5 mm Hex, Ø1/2" Aluminum Post 8-32 Setscrew 1/4"-20 Tap L=1",2",4", SM1 Lens Tube 1.00" and 0.50" Thread Depth One Retaining Ring Included, SM1 (1.035"-40) Coupler External Threads 0.5" Long

Contact angle measurements: The contact angle, θ, of anisole to AAO-based template was measured with the Drop Shape Analysis (DSA) 100S Krüss Tensiometer, GmbH, Germany.

Atomic Force Microscopy (AFM). Surface topography and mechanical parameters (adhesion) were measured using a NanoWizard®3 BioScience (JPK Instruments, Berlin, Germany) AFM. Images were acquired using ultra-sharp Si tips with a diamond-like spike with different force constants (3 – 5 N/m) and the resonant frequencies (75 – 150 kHz). Statistical analysis and mechanical parameters were estimated using JPK software and Gwyddion package. These investigations were performed along the cross-section of empty membranes.

Procedures

Prior to the photo-ATRO process, both commercially-available and self-made mesoreactors were purified using the same purification procedure. First, mesoreactors were washed with different organic and inorganic solvents (water, chloroform, THF, acetone) to remove impurities formed during the templates production. Importantly, the resulting filtrates were analyzed by NMR until the impurities have been completely removed. Next, to evaporate solvents from the mesochannels, the templates were dried under vacuum at oven at 100 °C within 24 h.

Photo-ATRP within mesoporous templates

Example of reaction with $[MMA]_0/[EBiB]_0/[PC1]_0=100/1/0.1$:

MMA (0.75 mL, 7 mmol), EBiB (10.3 μl, 0.07 mmol), PC1 (4.65 mg, 0.007 mmol), and anisole (0.15 ml) were placed in a Schlenk flask. The solution was purified by three freeze-pump-thaw cycles and purged under nitrogen. The reaction mixture was transferred into a flask together with the alumina templates. Then, the whole system was maintained at T=15 °C under vacuum (10^{-2} bar) for 1h to allow reagents to flow into the nanocavities. After the infiltration was completed, the surface of templates was dried mechanically with a paper towel to remove the excess of the reaction mixture, transferred to the chamber equipped with a UV diode and left under light irradiation (λ=365 nm). The polymerization was stopped after 3h by turning off the light source. First, the polymer was isolated from the template by immersing in the $CDCl_3$ and left to wash for 1h using ultrasonic bath in order to determine the MMA consumption by ^1H NMR. Next, after the template was removed, the solvent was evaporated and the polymer was precipitated into cold methanol, filtrated and dried under vacuum to constant mass. Purified PMMA was washed with cold methanol followed by its dissolution in DMF to perform SEC-LALLS measurements (inserts for SEC vials were used).

A similar procedure was used for PC2 mediated reactions except for the use of a different solvent i.e., DMF. The setup for confined photo-ATRP experiments is presented in Fig. S1.

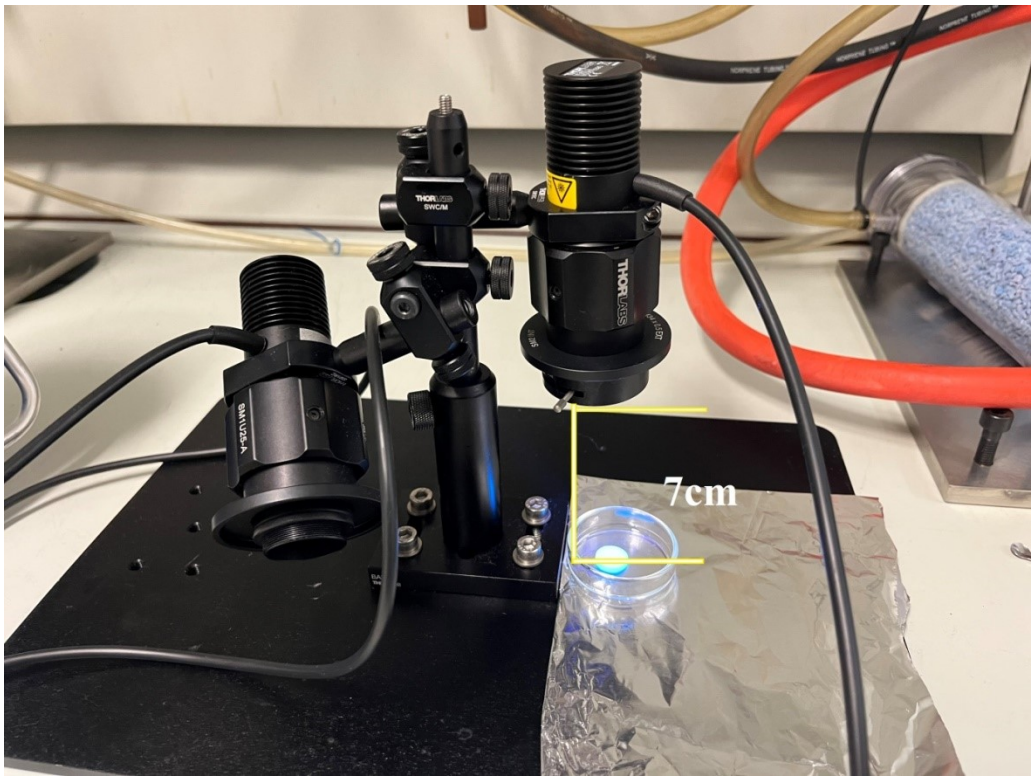

Fig S1. The setup for confined photo-ATRP experiments.

Photo-ATRP at the macroscale

Example of reaction with $[MMA]_0/[EBiB]_0/[PC2]_0=100/1/0.1$:
MMA (0.75 mL, 7 mmol), EBiB (10.3 µl, 0.07 mmol), PC2 (1.78 mg, 0.007 mmol), and DMF (0.15 ml) were placed in a Schlenk flask. The solution was purified by three freeze-pump-thaw cycles and purged under nitrogen within 15 min. The reaction mixture was transferred into a vial (3 ml) and left under light irradiation (λ=365 nm). The polymer was isolated by precipitation into cold methanol and dried under vacuum to a constant mass.

A similar procedure was used for PC1 mediated reactions except for the use of a different solvent i.e., anisole.

Chain-extension experiments with glicydyl methacrylate

Example of reaction with $[GMA]_0/[PMMA\text{-}Br]_0/[PC1]_0=200/1/0.1$:
GMA (0.23 mL, 1.68 mmol), PMMA-Br sample no 1 (0.03456, 0.00864 mmol), PC1 (0.54 mg, 8.8×10^{-4} mmol), and DMSO (0.21 ml) were placed in a Schlenk flask. The solution was purified by three freeze-pump-thaw cycles and purged under nitrogen within 15 min. The reaction mixture was transferred into a vial (3 ml) and left under light irradiation (λ=365 nm) for 6 h (conv. = 54%). The polymer was isolated by precipitation into cold methanol and dried under vacuum to a constant mass. A similar procedure was used for PC2 mediated reaction.

Results and discussion

The emission-absorption profiles of PCs with the specification of the applied light source

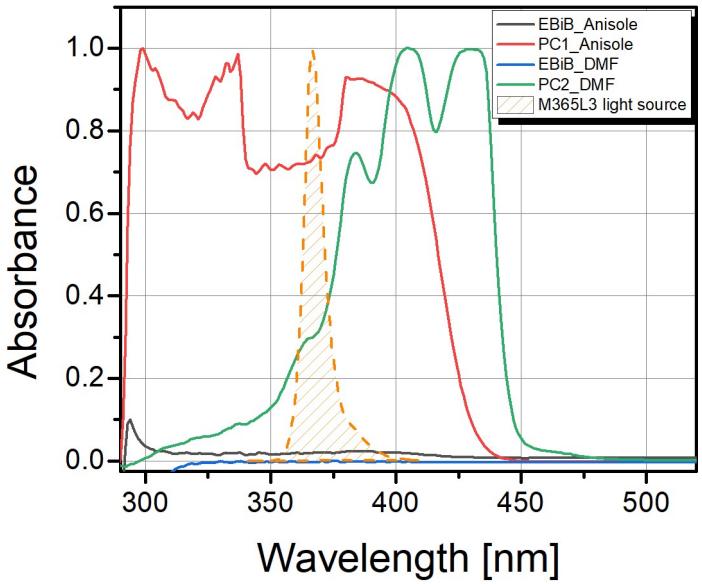

Fig. S2. The UV-vis absorption spectra of both examined systems (0.01 mmol/ml). Emission spectrum of the used light source 365 nm reprinted from the Webpage of the producer https://www.thorlabs.com/locations.cfm

SEC-LALLS measurements

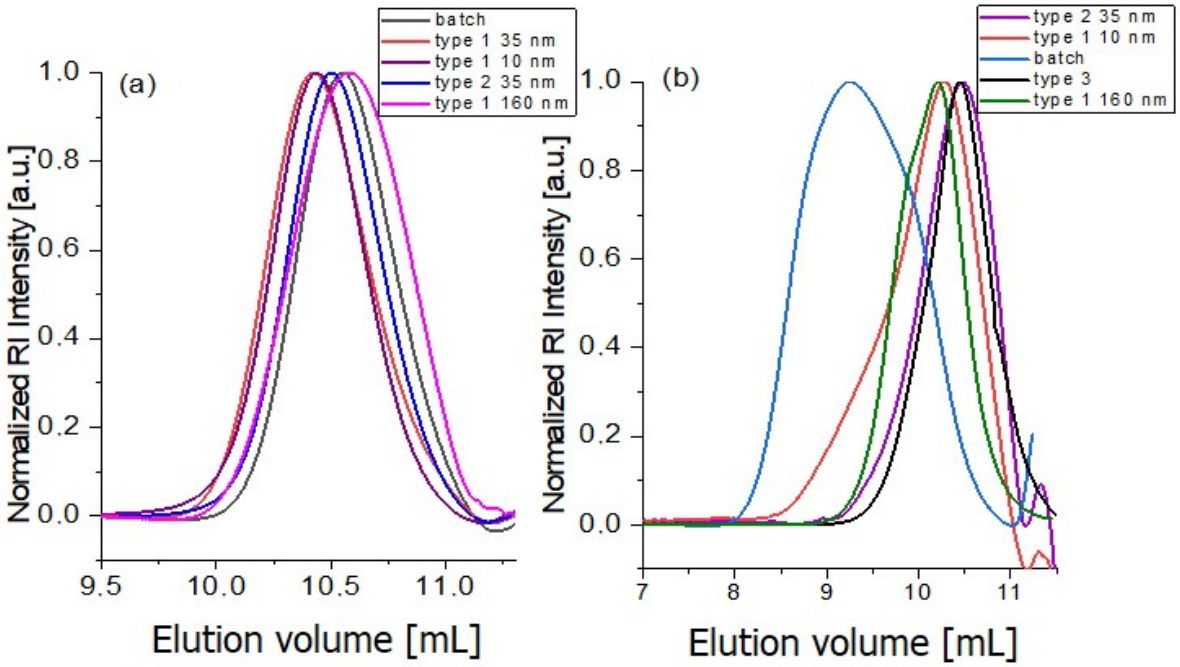

Fig. S3. Representative SEC-LALLS traces of PMMAs produced via (a) PC1-mediated *O*-ATRP, and (b) PC2-mediated *O*-ATRP.

The symmetric and monomodal SEC-LALLS traces of PMMA produced *via* PC1-mediated *O*-ATRP reflect a more controllable process compared to the PC2-mediated one. Despite very broad trace recorded for the PC2-mediated batch system, some of the other samples recovered from the mesoreactors reveal slight tailing at both lower (see sample recovered from type 3 template) or higher molecular weight (see type 1, 160 nm).

Results of chain-extension experiments with glycidyl methacrylate (GMA). Sample 13 (PC1): PMMA-*bl*-PGMA M_{nth}=19.4 kg/mol, $M_{nSEC\text{-}LALLS}$=21.9 kg/mol, Đ=1.29, dn/dc=0.043; Sample 14 (PC2): PMMA-*bl*-PGMA M_{nth}=94.7 kg/mol, $M_{nSEC\text{-}LALLS}$=111.0 kg/mol, Đ=1.65, dn/dc=0.045. As shown in Fig. S4 copolymer produced with PC1 has symmetric SEC-LALLS trace and moderate dispersity, whereas that obtained in PC2 reveals an unsymmetric trace with tailing at low MW.

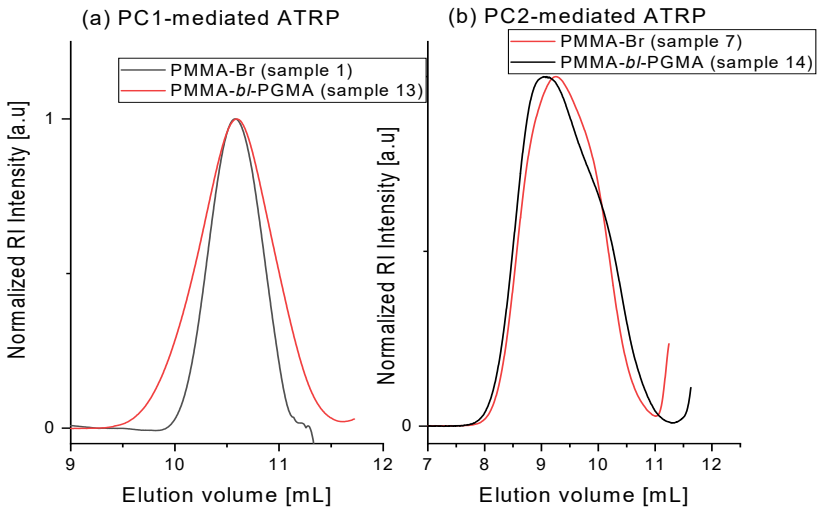

Fig. S4. SEC-LALLS traces of PMMA-*bl*-PGMA copolymers produced via (a) PC1-mediated *O*-ATRP, and (b) PC2-mediated *O*-ATRP.

NMR analysis

The representative ^{1}H NMR spectrum taken from PC1-mediated process is presented in Fig S5. Percentage of reacted initiator was calculated using the integrations of methylene protons of the unreacted initiator (sharp triplet at 1.28 ppm), and the integration of the methylene protons corresponding to the consumed initiator (1.22 ppm). For PC1-mediated processes 85-91% of polymer chains were bromine-ended, while for PC2-mediated process only 5-10%.

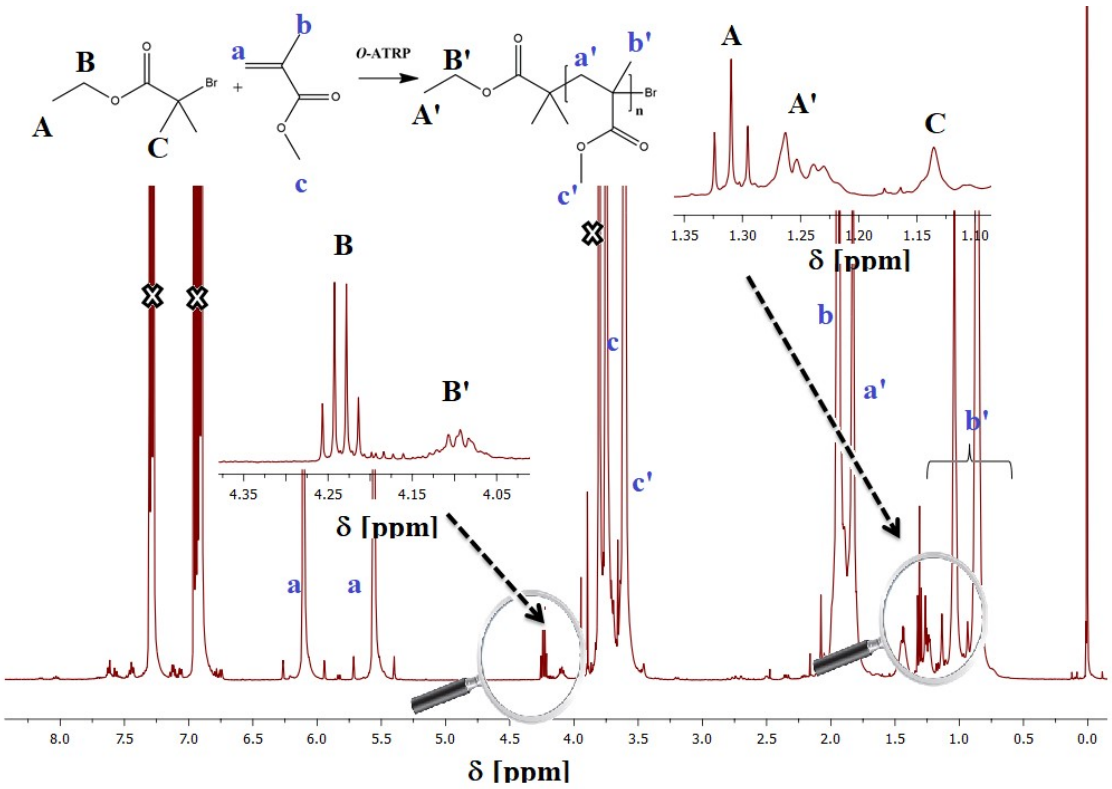

Fig. S5. Representative ^{1}H NMR spectrum taken from the polymerization mixture for MMA *O*-ATRP mediated by PC1 organophotocatalyst.

Determination of PMMA tacticity from ^{1}H NMR

The tacticity of PMMA (prepared via controlled PC1-mediated process) was calculated by ^{1}H NMR integrating the intensities of α-CH_3 peaks at 1.35-1.12, 1.12-0.95, and 0.95-0.78 ppm for the isotactic (mm), atactic (mr), and syndiotactic (rr) triads, respectively.

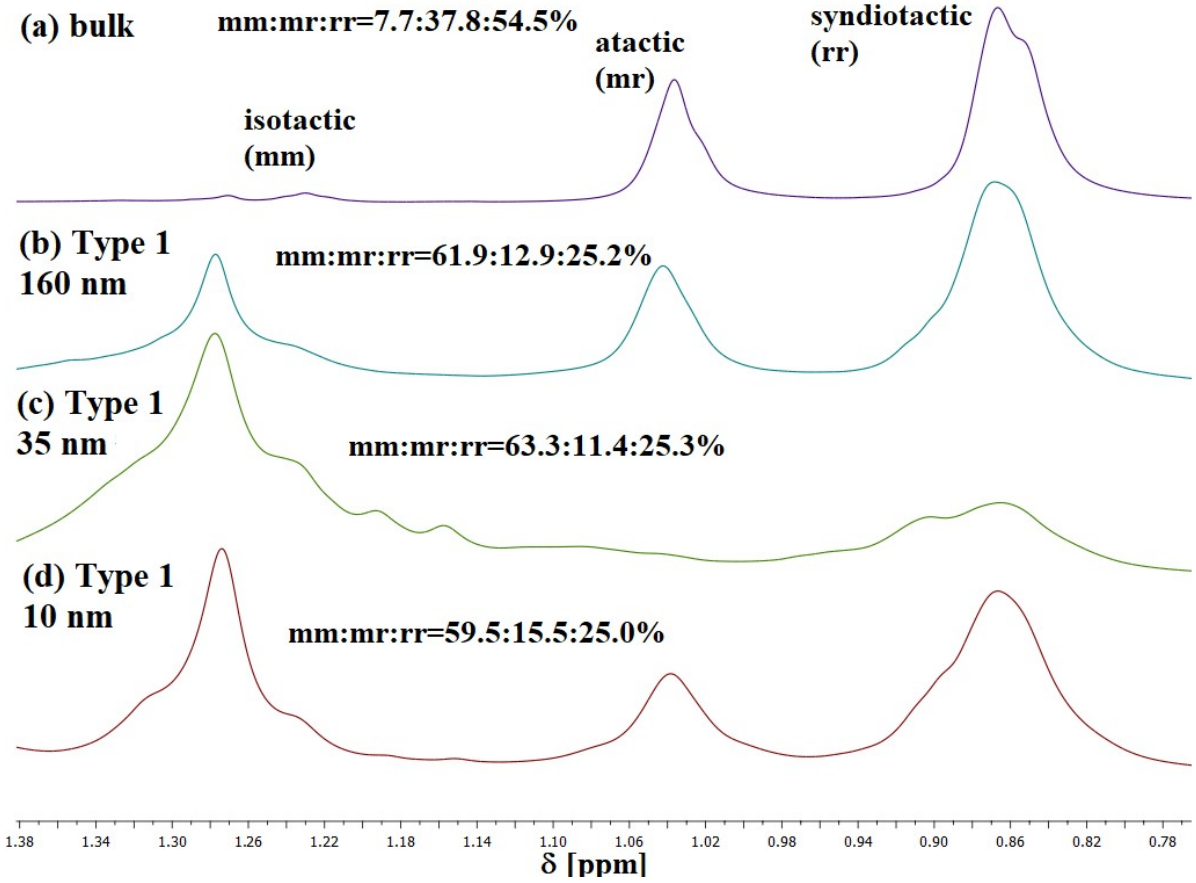

Fig. S6. ^{1}H NMR spectra of α-CH_3 of PMMA in $CDCl_3$ for PMMA synthesized by PC1-mediated *O*-ATRP at the macroscale and nanoscale.

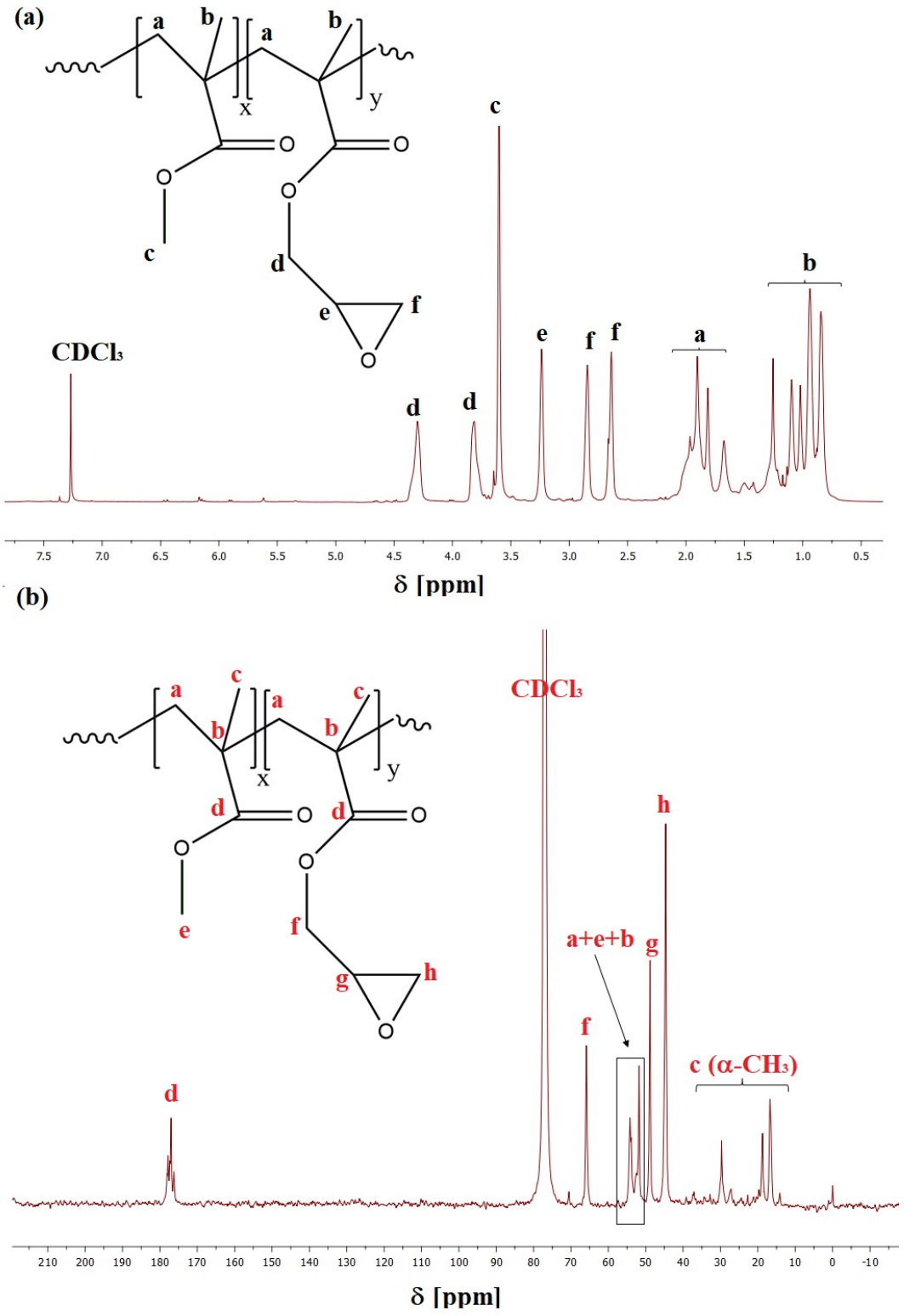

Fig. S7. (a) ^{1}H NMR and (b) ^{13}C NMR spectra of PMMA-*bl*-PGMA synthesized by PC1-mediated photo-ATRP ($CDCl_3$, 600 MHz)

FT-IR analysis

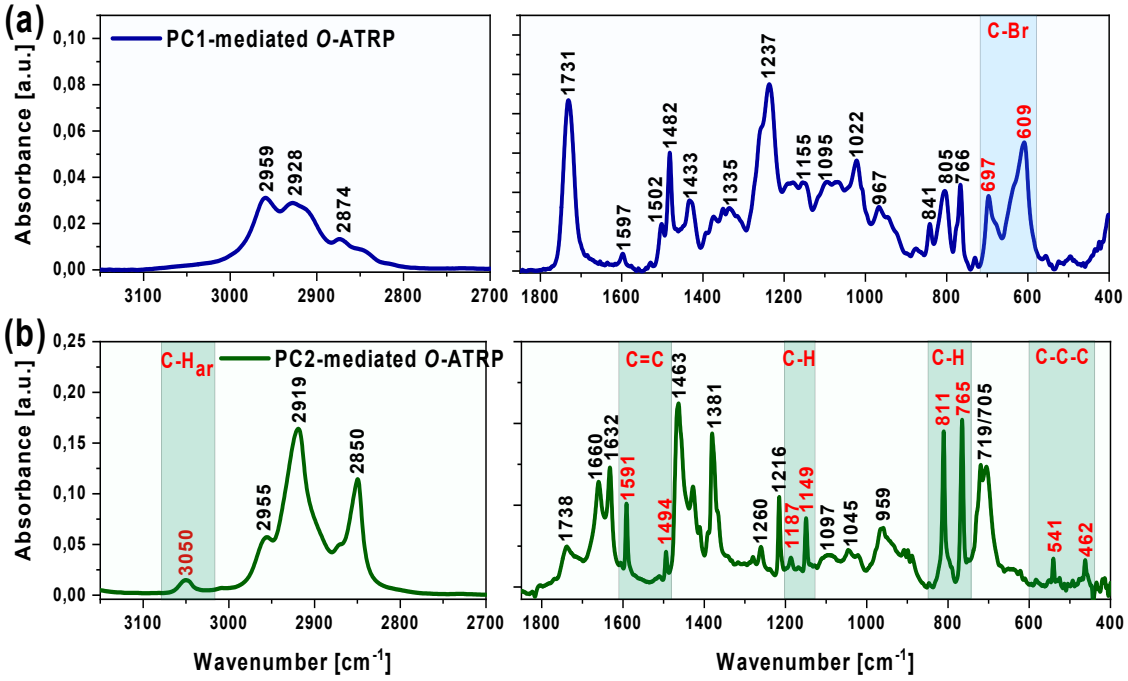

Fig. S8. FTIR spectrum of (a) PMMA prepared via PC1-mediated *O*-ATRP and (b) PMMA prepared by PC2-medaited *O*-ATRP measured in the spectral range of (left) 3150-2700 cm^{-1} and (right) 1850-400 cm^{-1}.

FTIR spectroscopy was used to identify changes in the chemical structure of PMMA using two different PCs. Generally, the vibrational frequencies observed in the FTIR spectrum of the analyzed PMMA sample are very similar to those observed for the PMMA polymer in our previous paper.[4] As shown in Figure S8a a broad band appearing from 2800 cm^{-1} to 3100 cm^{-1} (2874, 2928, and 2959 cm^{-1}) is due to the asymmetric and symmetric C-H stretching vibrations of the methyl carboxyl, chain methyl pendant, and the main chain methylene groups of PMMA polymer.[5] A strong peak at 1731 cm^{-1} is attributed to the C=O stretch of the ester groups. The absorption signals appearing at 1482 and 1433 cm^{-1} are related to the asymmetric bending vibrations of ($C\text{-}CH_2$) and ($C\text{-}CH_3$) groups, respectively. The bands in the region from 1350 to 1300 cm^{-1} correspond to the CH_2 wagging vibration with considerable contributions from the backbone and side-chain C-C stretching vibrations.[6] Then, the C-O-C stretching vibrations of ester groups are located at 1237, 1178, and 1155 cm^{-1}. Moreover, the bands occurring below 1000 cm^{-1} correspond to the C-C skeletal and C-H rocking vibrations. It is noteworthy that the peaks with strong intensity at 697 and 609 cm^{-1} (highlighted in blue in Fig. S8a can be ascribed to the C-Br bond formation as bromine compounds absorb in the region 750-485 cm^{-1} due to the C-Br stretching vibrations. More than one C-Br stretching band can be due to the different possible rotational isomeric configurations available (the trans- form absorbs at higher frequencies than the gauche-form). [7] In the spectrum of PMMA produced via PC2-mediated *O*-ATRP (see Fig. S8b) some of the bands originating from PMMA molecule is slightly shifted in relation to the corresponding

bands appearing in the spectrum of PC1-mediated one. Moreover, new bands of weaker intensity occurring at 3050 cm^{-1} (aromatic C-H stretching); 1606, 1591, 1510, 1494 cm^{-1} (aromatic C-C stretching); 1187, 1149, 1045 cm^{-1} (C-H in plane bending and/or C-H rocking); 889, 811 and 765 cm^{-1} (C-H out-of-plane bending); 583, 541 and 462 cm^{-1} (C-C-C out-of-plane bending) in the spectrum of PC2-mediated experiment corresponds to the vibrations of groups belonging to perylene molecules incorporated in PMMA skeleton (highlighted in green in Fig. S8b. In addition, the band at 2850 cm^{-1} (aliphatic C-H stretching) is characterized by a much greater intensity in the IR spectrum of PC2-mediated process than in the sample produced via PC1-mediated process. These facts indicate that PMMA polymerization process using perylene-based catalyst is less controlled than catalyzed by PC1. As a result, perylene molecules are partly incorporated into polymer prepared by PC2-mediated process, and the CH_3 groups appear as end groups. These results are in line with those calculated from ^1H NMR analyses. The percentage of bromine-chain end for PC2-mediated process was very low reaching maximum value 10%.

The examination if syndiospecific propagation is governed by the entropic or enthalpic factor

According to the absolute reaction rate theory the ratio between the fraction of meso and raceme diads (P_m and P_r respectively) can be related to the differences in activation enthalpy $\Delta H_{act}^{\ i} - \Delta H_{act}^{\ s}$ and the entropy $\Delta S_{act}^{\ i} - \Delta S_{act}^{\ s}$ between isotactic and syndiotactic propagations:

$$\ln \frac{P_m}{P_r} = \frac{\Delta S_{act}^{\ i} - \Delta S_{act}^{\ s}}{R} - \frac{\Delta H_{act}^{\ i} - \Delta H_{act}^{\ s}}{RT}.$$

The ratio between P_m and P_r can be estimated on the basis of the observed triad fraction, i.e, $\frac{P_m}{P_r} = ([mm] + [mr]/2)/\,([rr] + [mr]/2)$ (see Table S1). The results are presented in Fig. 1 (main manuscript) and fitted by the linear functions, of which parameters are presented in Table S2.

Table S2. Values estimated on the basis of the absolute reaction rate theory

System	T [K]	mm	mr	rr	$\Delta H_{act}^{\ i} - \Delta H_{act}^{\ s}$ $[kJ/mol]$	$\Delta S_{act}^{\ i} - \Delta S_{act}^{\ s}$ $[J/mol \cdot K]$	$P_{mr} + P_{rm}$
BULK	298	7.7	37.8	54.5	3.5 ± 1.7	3.3 ± 5.4	0.97
	308	10.6	32.3	57.4			0.82
	318	10.5	38.1	51.4			0.92
	333	10.7	36.7	52.6			0.89
TYPE 1 160 mm	298	61.9	12.9	25.2	3.8 ± 2.7	18.9 ± 9.0	0.30
	308	61.3	9.8	28.9			0.22
	318	64.2	12.8	23.0			0.31
	333	66.2	9.1	24.7			0.22
TYPE 1 35 mm	298	63.3	11.4	25.3	-4.8 ± 2.6	-9.4 ± 8.3	0.27
	308	58.5	16.9	24.6			0.38
	318	63.3	10.8	25.9			0.25
	333	55.6	16.1	28.3			0.38
TYPE 1 10 nm	298	59.5	15.5	25.0	-3.3 ± 2.5	-5.7 ± 8.3	0.35
	308	55.3	14.9	29.8			0.32

	318	58.0	11.0	31.0			0.24
	333	54.4	17.9	27.7			0.39
TYPE 2	298	41.5	26.8	31.7	11.4 ± 4.2	40.5 ± 9.4	0.54
	308	55.3	14.9	29.8			0.32
	318	52.1	21.9	26.0			0.47
	333	53.2	28.4	18.4			0.65
TYPE 3	298	23.8	40.6	35.6	27.4 ± 3.2	89.0 ± 10.4	0.82
	308	35.2	28.1	36.7			0.56
	318	54.1	16.2	29.7			0.34
	333	62.8	15.1	22.1			0.36

Additionally, we check if the propagation of monomer adds fulfils the Bernoulian or 1st-order Markov statistics. It is worth to note that previous studies demonstrated that Bernoulian statistics successfully predicts PMMA tacticity produced via bulk FRP.[8] However, Uemura[9], and Simon[10] groups reported that this model does not work for confined polymerization processes, and in such systems 1st-order Markov model can be successfully applied. Since the Bernoulian model is regarded as zero-order Markov model, we next calculate the crucial for Markov models quantities. As one can see in Table S1 the propagation of monomer adds for all studied herein systems cannot be described by the Bernoulian statistics. The best results are registered for bulk systems however even then they evidently deviate from the unity. Hence, the propagation of monomer adds should be described by 1st-order Markov statistics model rather than Bernoulian model.

Contact angle measurements

The description of the instrument and procedures has been presented previously.[11]

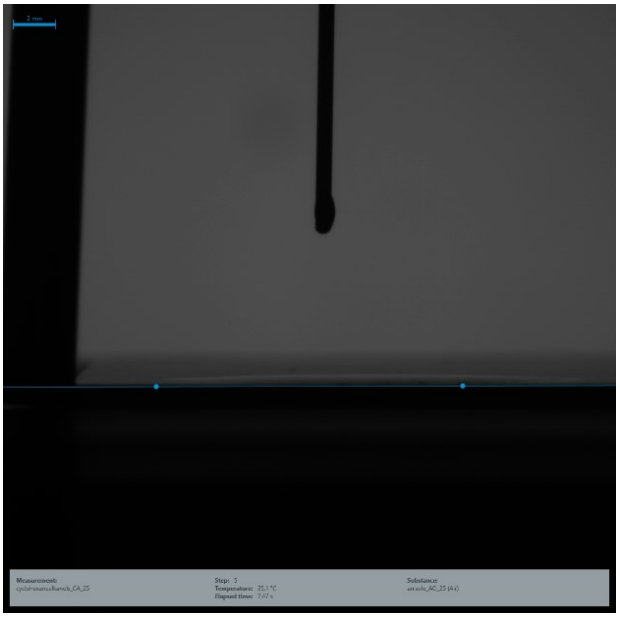

Fig. S9. Photo taken while measuring the contact angle of anisole to the AAO surface.

AFM measurements

Using ultra sharp tip we were able to measure the inner roughness parameter of the empty pores in nanoreactors in nanoscale. In order to do that, we have taken the nanoreactor and broke it along the long axis of the pores. This allowed of access from the top. Next, for each AFM image we have masked the regions of the inner side of the pore, allowing us to get the RMS values of the pore surface. The schematic of a pore structure, along with the AFM approach is shown in Fig. 2 (main manuscript). Typical data of topography is also shown, along with the 3d image of the surface. The red color shows the masked region, which is the inner surface of the pores, that was included into the analysis. We have gathered data from a number of images, getting enough information to obtain statistically valid differences. We have calculated RMS values along vertical lines using only the data from the pore internal wall (the masked regions). Thus, we were able to obtain a linear RMS (l-RMS), that is not influenced by the horizontal high changes (pores curvature) and can be used for comparison between nanoreactors.

---

[1] A. Brzózka, D. Szeliga, E. Kurowska-Tabor, G. D.Sulka, *Mater. Lett.* **2016**, *174*, 66–70

[2] M.Tarnacka, M.Wojtyniak, A. Brzózka, A. Talik, B. Hachuła, E. Kamińska, G.D. Sulka, K. Kaminski, M.Paluch, *ACS Nano*, **2020**, *20*, 5714–5719

[3] https://www.inredox.com/technology/anodic-aluminum-oxide/

[4] R. Bernat, P. Maksym, M. Tarnacka, A. Szelwicka, R. Bielas, M. Wojtyniak, K. Balin, B. Hachuła, A. Chrobok, M. Paluch and K. Kamiński, *Polym. Chem*., 2021, **12**, 1105-1113.

[5] F. Namouchi, H. Smaoui, N. Fourati, C. Zerrouki, H. Guermazi and J. J. Bonnet, *J. Alloys Compd*., 2009, **469**, 197-202.

[6] J. Dybal and S. Krimm, *Macromolecules*, 1990, **23**, 1301-1308.

[7] G. Socrates, Infrared and Raman Characteristic Group Frequencies: Tables and Charts, 3rd Edition, John Wiley & Sons Ltd, Chichester, 2001.

[8] F. A. Bovey, G. V. D. Tiers, **1960**, *XLIV*, 173–182

[9] T. Uemura, Y. Ono, K. Kitagawa, S. Kitagawa, *Macromolecules* **2008**, *41*, 87–94

[10] H. Y. Zhao, Z. N. Yu, F. Begum, R. C. Hedden, S. L. Simon, *Polymer (Guildf).* **2014**, *55*, 4959–4965.

[11] J. Feder-Kubis, M. Geppert-Rybczynska, M. Musiał, E. Talik, and A. Guzik, *A Physicochem. Eng. Asp*. **2017**, *529*, 725–732